Journal of Vibration and Control
XX(X):1–12

DOI: 10.1177/ToBeAssigned
www.sagepub.com/
SAGE

Optimal fluid passageway design methodology for hydraulic engine mounts considering both low and high frequency performances

Yuan Li, Jason Zheng Jiang and Simon A. Neild

Abstract

This paper investigates the potential for improving the performance of hydraulic engine mounts through fluid passageway designs. In previous studies, a few simple inertia track designs have been investigated with moderate improvements obtained. However, there are countless alternative design possibilities existing; while analysing each one of them in turn is impracticable. To this end, this paper introduces a systematic methodology to optimise fluid passageway designs in a hydraulic engine mount. First beneficial fluid passageway configurations are systematically identified using a linearised low-frequency model that captures the relative displacement transmissibility. A nonlinear model is then used to fine-tune the fluid passageway designs for the low-frequency transmissibility improvement, and also for the assessment of high-frequency dynamic stiffness performance. The obtained beneficial designs present performance advantages over a wide frequency range. The design approach introduced in this study is directly applicable to other engine mount models and performance criteria.

Keywords

Fluid passageway, hydraulic engine mount, network topology, transmissibility, dynamic stiffness

Introduction

Vehicle engine mounts must be designed to mitigate undesirable vibrations over a wide frequency range, due to low-frequency road unevenness and high-frequency engine excitations (Singh et al. 1992). The mount needs to be "soft" to isolate the car body from engine excitations in the frequency range 25–250 Hz, but "stiff" when low-frequency high-amplitude road inputs, typically 0–30 Hz, are transmitted

Faculty of Engineering, University of Bristol, UK

Corresponding author:
Jason Zheng Jiang, Faculty of Engineering, Queen's Building, University Walk, Bristol BS8 1TR, UK
Email: z.jiang@bristol.ac.uk

Prepared using sagej.cls *[Version: 2017/01/17 v1.20]*

through the mounts (Singh et al. 1992). To achieve this frequency-dependent behaviour, passive rubber-hydraulic mounts were proposed to provide superior dynamic properties over those of rubber mounts (Kim and Singh 1995). The design of active or semi-active engine mounts becomes more popular recently, see (Mansour et al. 2011; Fakhari et al. 2015) as examples. However, passive mounts are still widely used due to the design simplicity and low cost.

Research efforts were made to model passive hydraulic mount as a linear lumped-parameter model (Singh et al. 1992). Since then, frequency and amplitude-dependent nonlinear features, including chamber compliance (Geisberger et al. 2002), flow resistance (Wang et al. 2010) and decoupler switching dynamics (Tiwari et al. 2003), have been considered. Geisberger et al. (2002) developed a nonlinear lumped-parameter model which captures both low and high frequency behaviour and could be adopted for design purposes. While finite element analysis has been used to study mount dynamics in detail (Guo et al. 2017), lumped-parameter models are commonly employed to analyse and design hydraulic mounts due to their direct link with mount properties (Marzbani et al. 2014).

To improve the performance of passive engine mounts, attempts have been made to alter existing designs (Marzbani et al. 2014), such as rubber stiffness, piston area, fluid inertia, volumetric stiffness and damping. Altering the mount's interior configuration to improve flow motion has also been considered. Zhang and Shangguan (2006) investigated the low-frequency dynamic responses of hydraulic mounts with multiple parallel inertia tracks. Barszcz et al. (2012) considered adding an orifice to create a broadband device and Tikani et al. (2011) employed an inner and outer inertia tracks to reduce the peak dynamic stiffness. All these studies focused on specific fluid passageway designs. While improvements were identified, it is likely that further benefits can be achieved given countless alternative design possibilities, but to analyse them all one by one is unrealistic.

The contribution of this paper is to introduce a systematic design methodology for investigating a range of fluid passageway designs. Furthermore, in contrast to many previous studies on engine mounts, this paper considers low and high-frequency design requirements together. This paper is organised as follows. A nonlinear model of a conventional hydraulic mount reported in Geisberger et al. (2002) is first discussed and two performance criteria, relative displacement transmissibility under low-frequency road disturbance and dynamic stiffness amplitude under high-frequency engine excitation, are proposed. Then an optimisation procedure using a linearised low-frequency model is introduced to consider a wide range of fluid passageway arrangements (inertia track and orifice). Two configurations using an inertia track and orifice are found to be beneficial. Nonlinear optimisations using these two designs and a high-frequency performance constraint allow the optimal physical geometries to be obtained. Low-frequency relative displacement transmissibility improvement, while constraining high-frequency dynamic stiffness, are identified. Finally, some conclusions are drawn in the last section.

Passive hydraulic engine mount model and performance criteria

In this section, a nonlinear model of a typical hydraulic engine mount (Geisberger et al. 2002) that captures the mount dynamics over a wide frequency range is considered. The parameter values used in the model were experimentally validated in (Geisberger et al. 2002). Note that flow condition and rubber characteristic assumptions are made in this model. Both low and high-frequency performance criteria are then proposed.

Nonlinear engine mount model

For a conventional hydraulic engine mount, there are two fluid-filled chambers, which are connected via a spiral inertia track and a typical free decoupler, as shown in Figure 1(a). A lumped-parameter model (Geisberger et al. 2002) is used to predict the mount behaviour in both low and high frequencies. A low-frequency base excitation x_s is first considered to formulate the overall equations of motion, with the resulting engine displacement represented by x_e.

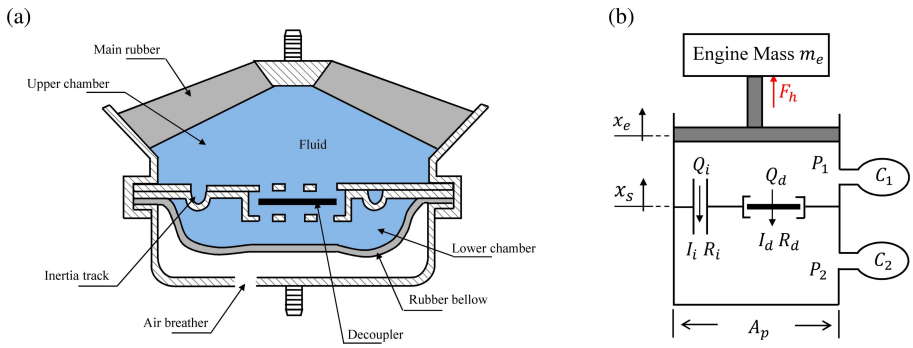

Figure 1. (a) Cross-section schematic of a typical hydraulic passive engine mount (reproduced from Geisberger et al. (2002)), (b) the lumped-parameter hydraulic model with chassis excitation x_s and resulting engine motion x_e.

When a base excitation is applied, using the lumped-parameter hydraulic model in Figure 1(b) allows the continuity and momentum equations to be written as

$$C_1\dot{P}_1 = -A_p(\dot{x}_e - \dot{x}_s) - Q_i - Q_d, \tag{1}$$

$$C_2\dot{P}_2 = Q_i + Q_d, \tag{2}$$

$$P_1 - P_2 = I_i\dot{Q}_i + R_iQ_i, \tag{3}$$

$$P_1 - P_2 = I_d\dot{Q}_d + R_dQ_d, \tag{4}$$

where A_p is the piston area, C_1 and C_2 are the volumetric compliances of the upper and lower chambers, P_1 and P_2 are the pressure within upper and lower chambers, and Q_i and Q_d are the fluid flow rates through the inertia track and decoupler, respectively. Assuming the flow through the inertia track is laminar and the entrance loss is negligible, the inertia track is modelled by fluid inertia I_i and linear resistance R_i. The decoupler fluid inertia is represented by I_d and a nonlinear decoupler resistance R_d

$$R_d = R_d^{'} + R_0 e^{(X_d/X_0)\arctan(Q_d/Q_0)}, \tag{5}$$

is used to model the switching mechanism. $R_d^{'}$ is the linear resistance and the second term represents an additional resistance to control the decoupler switching function. The decoupler position is $X_d = V_d/A_d$, where A_d is the measured decoupler area, X_0 is the decoupler cage height and Q_0 is used to produce a

crisp switching response. The flow volume for inertia track and decoupler are represented by $V_i = \int Q_i dt$ and $V_d = \int Q_d dt$, respectively.

Table 1. Parameters values used in the analysis

Symbol	Parameter	Value
A_p	Effective piston area	2.5×10^{-3} m^2
c_r	Upper chamber damping	300 Ns/m
C_1	Upper chamber compliance	3.0×10^{-11} m^5/N
C_2	Lower chamber compliance	2.6×10^{-9} m^5/N
I_d	Fluid inertia in decoupler	7.5×10^4 kg/m^4
I_i	Fluid inertia in inertia track	3.8×10^6 kg/m^4
k_r	Upper chamber stiffness	2.25×10^5 N/m
P_0	Pressure normalised constant	10 N/m^2
Q_0	Flow normalised constant	1.0×10^{-9} m^3/s
$R_d^{'}$	Linear fluid resistance in decoupler	1.17×10^7 kg/(s·m^4)
R_i	Fluid resistance in inertia track	1.05×10^8 kg/(s·m^4)
R_0	Nonlinear resistance constant in decoupler	1.0×10^{-4} kg/(s·m^4)
X_{dmax}	Half decoupler cage height	5.3×10^{-4} m
X_0	Decoupler position control constant	2.62×10^{-5} m
X_1	Decoupler switching function shape control constant	1.0×10^{-9} m
ρ	Fluid density	1.028×10^3 kg/m^3

The transmitted force F_T from the mount to the chassis or engine is

$$F_T = m_e \ddot{x}_e = -k_r(x_e - x_s) - c_r(\dot{x}_e - \dot{x}_s) + F_h, \tag{6}$$

$$F_h = (A_p - A_{dfnc})(P_1 - P_2) + A_p P_2 + A_d R_d Q_d, \tag{7}$$

$$A_{dfnc} = \frac{A_d}{2} - \frac{A_d}{\pi} \arctan\left(\frac{\frac{2}{\pi} X_d \arctan(\frac{\Delta P}{P_0}) - X_{dmax}}{X_1}\right). \tag{8}$$

Here k_r and c_r are the upper chamber stiffness and damping, F_h represents the total force generated by the flow in the mount and the engine mass m_e is assumed to be 60 kg. The effective piston area is the total piston area A_p minus A_{dfnc} - the decoupler area with respect to the plate position and pressure differential. P_0 and X_1 are constants used to normalise the function and control the switching function shape. X_{dmax} is half the decoupler cage height. Readers can refer to (Geisberger et al. 2002) for details of the modelling process. The system parameters used in this analysis have been summarised in Table 1. The default inertia track geometry, with length $L_i = 0.212$ m and cross-section area $A_i = 5.72 \times 10^{-5}$ m, are used as a reference for the following discussion.

Performance criteria

Based on the design requirements, two performance criteria in line with previous studies, such as (Foumani et al. 2004; Geisberger et al. 2002), are proposed here, one is the low-frequency relative displacement transmissibility due to the road roughness and the other the high-frequency dynamic stiffness. These criteria, used as the cost function and constraint for the optimisation, serve as examples

to demonstrate the effectiveness of the proposed approach. This approach is independent on the selection of cost functions and constraints, i.e., other cost functions and constraints can be directly used for the optimisation while following the same design approach.

Low-frequency relative displacement transmissibility One of the most significant low-frequency excitation sources is road disturbance. Under this excitation, the relative displacement transmissibility $|T_d|$ is an important criteria (Foumani et al. 2004) as it is linked to both chassis-engine contact and the service life of connecting parts. It is represented by

$$|T_d| = \frac{|x_e - x_s|}{|x_s|}, \tag{9}$$

where $x_s = \mathrm{X}_{\boldsymbol{ms}} \sin(2\pi f t)$, the low-frequency excitation amplitude $\mathrm{X}_{\boldsymbol{ms}} = 1.0$ mm and $0 < f \leq 30$ Hz (Colgate et al. 1995). The frequency response of $|T_d|$ calculated using a time-domain simulation is shown in Figure 2(a). Here the maximum $|T_d|$ over the low frequency range for the default mount is 3.45.

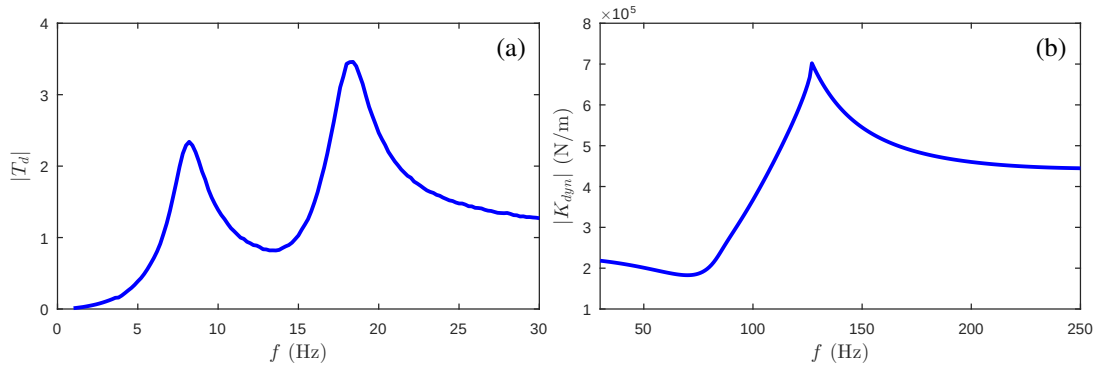

Figure 2. (a) The default low-frequency $|T_d|$ under a base excitation $x_s$and (b) high-frequency $|K_{dyn}|$ performance under an engine excitation x_e using the nonlinear model.

High-frequency dynamic stiffness The engine mount experiences high-frequency small-amplitude excitations from the engine. It is desirable to have lower transmitted force, hence less vibrations, to the chassis. Since the transmitted force from engine excitation is determined by the mount dynamic stiffness, it is important to make sure the dynamic stiffness is below a pre-determined level. Hence in this work, the maximum high-frequency dynamic stiffness amplitude of the engine mount, which is represented by $\max(|K_{dyn}|)$, is chosen as the second performance criteria. A fixed base is assumed and an engine excitation x_e is applied. We take

$$|K_{dyn}| = \frac{|F_T|}{|x_e|}, \tag{10}$$

where $x_e = \mathrm{X}_{\boldsymbol{me}} \sin(2\pi f t)$, the high-frequency excitation amplitude $\mathrm{X}_{\boldsymbol{me}} = 0.05$ mm and $30 < f \leq 250$ Hz (Geisberger et al. 2002).

Figure 2(b) shows the $|K_{dyn}|$ for the default engine mount using the nonlinear model, with $\max(|K_{dyn}| = 701985)$N/m. From time-stepping simulations, it is found that over a small frequency

region spanning the peak in $|K_{dyn}|$, the time-domain steady-state responses are multi-valued and sensitive to the initial conditions (Li 2018; Geisberger et al. 2002). Numerical continuation, a technique designed to analyse nonlinear behaviour, was used to verify the time-stepping results (Li 2018). It has been observed that although continuation method is more accurate, the high-frequency responses obtained with two methods are similar while the low-frequency dynamics stay the same (Li 2018). Hence for better optimisation efficiency, time-stepping will be used for the following investigation.

Optimisations of fluid passageway designs

The inertia track and orifice are considered as two fluid passageway types in this work. A systematic identification procedure for beneficial fluid passageway layouts using a low-frequency linearised model is introduced first in this section. This procedure neglects the decoupler dynamics and adopts a linear orifice model, in line with previous studies exampled by (Zhang and Shangguan 2006; Foumani et al. 2004). These configurations which provide significant benefits in reducing the maximum low-frequency relative displacement transmissibility are proposed. Fine-tuning of these configurations is then carried out using time-stepping simulations in MATLAB considering the dynamics of decoupler and a nonlinear orifice, along with a performance constraint on the high-frequency $|K_{dyn}|$. The MATLAB command *patternsearch* and *fminsearch* are used for the optimisations carried out in the present work.

Beneficial layout identification using a low-frequency linearised model

To explore a range of fluid passageway designs systematically, a low-frequency linearised engine mount model is used. In this model the decoupler dynamics are excluded as its influence on the low-frequency performance is minor (Li 2018). The maximum relative displacement transmissibility, max($|T_d|$) over $0 < f \leq 30$ Hz (see Equation (9)), is chosen as the objective function for the optimisations. Using the linearised model, the default max($|T_d|$) is 3.64.

The hydraulic representations of the inertia track and orifice considered here are shown in Table 2. The inertia track is modelled as a long capillary tube with circular cross-section shape, allowing the inertance I_i and damping R_i to be expressed as

$$I_i = \rho \frac{L_i}{A_i}, \quad R_i = \frac{128 \mu L_i}{\pi {d_i}^4}, \tag{11}$$

where μ is fluid dynamic viscosity, d_i is the diameter of the inertia track, $A_i = \pi {d_i}^2/4$ is its cross-section area. The optimisation parameters are defined to be the variations of inertia track geometry, which are the length L_i and cross-section area A_i, as

$$\delta_L = L_i/{L_i}^*, \quad \delta_A = A_i/{A_i}^*, \tag{12}$$

with $0.5 \leq \delta_L \leq 1.5$, $0.5 \leq \delta_A \leq 1.5$. Here $\pm 50\%$ constraints on inertia track geometry (Singh et al. 1992; Truong and Ahn 2010; Wang et al. 2014) are chosen. For this linear identification process, the orifice is modelled as a linear damping R_o (as shown in Table 2) with the optimisation parameter defined as variation of the damping comparing with the default inertia track damping ${R_i}^*$, as

$$\delta_o = R_o/{R_i}^*. \tag{13}$$

Using the transformation between hydraulic pressure-flow rate relationship to mechanical force-velocity one, equivalent mechanical networks of inertia track and orifice can be obtained, see Table 2 (Li 2018). The inertia track is equivalent to a mechanical inerter (Smith 2002) and damper in parallel. All the mechanical parameters (b_i, c_i and c_o, etc.) can be obtained by multiplying the corresponding hydraulic ones (I_i, R_i and R_o, etc.) with A_p^2, where A_p is the piston area. By using mechanical networks, any fluid passageway design can be expressed by linear mechanical transfer functions to be optimised. With a predetermined number of fluid passageways involved, all possible network topologies were established using the structure-immittance approach (Zhang et al. 2017). Note that Zhang et al. (2017) proposed the layouts based on components (spring, damper or inerter) while here we apply it in a device level (using inertia tracks and orifices).

Table 2. Beneficial hydraulic layouts and the equivalent mechanical networks using the linearised model [§].

Cases	Beneficial fluid passageways	Equivalent mechanical networks
Inertia track (H_1)	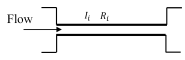	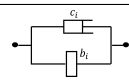
Orifice	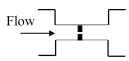	
H_{21}	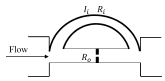	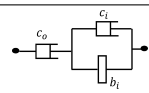
H_{22}	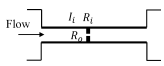	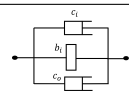
H_3	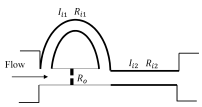	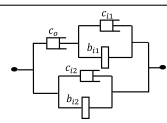
H_{41}	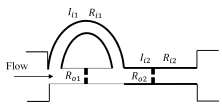	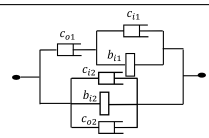
H_{42}	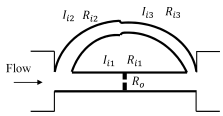	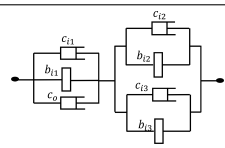

[§] Here thin lines used in a flow restriction are to stress its negligible length of the practical hydraulic passageway. All the mechanical parameters (b_i, c_i and c_o, etc.) can be obtained by multiplying the corresponding hydraulic ones (I_i, R_i and R_o, etc.) with A_p^2.

Based on the optimisations, the beneficial configurations consisting of up to four fluid passageways for minimising the max($|T_d|$) are shown in Table 2 and the corresponding parameter values summarised in Table 3. Note that the notation 'H_{mn}' is used to specify the hydraulic fluid passageway layout. The

subscripts 'm' and 'n' are used to specify the nth beneficial network of the ones consisting of m fluid passageways. Two improvement measures are used in the following discussions, Δ_d is a comparison with the default configuration, Δ_{do} is a comparison with the optimal solution using the default layout (one inertia track, H_1). From Table 3 it can be found that even though increasing the layout complexity leads to better performance, the improvement is marginal. Balancing these improvements with the added manufacturing complexity it is concluded that H_{21} and H_{22} are the most promising. These two layouts are now adopted for a more detailed study using a nonlinear model that captures the decoupler dynamics (allowing the high-frequency performance to be included) and a more realistic orifice model.

Table 3. Optimisation results using the linearised model.

Layouts	Performances			Parameter values (see Equations (12), (13))
	max($\|T_d\|$)	Δ_d (%)	Δ_{do} (%)	
Default	3.64	-	-	-
H_1 (optimal default)	2.34	35.71	-	$(\delta_L, \delta_A) = (0.5, 0.65)$
H_{21}	1.79	50.82	23.50	$(\delta_L, \delta_A) = (1.5, 1.03)$, $\delta_o = 5.07$
H_{22}	1.76	51.65	27.79	$(\delta_L, \delta_A) = (0.76, 1.22)$, $\delta_o = 1.85$
H_3	1.69	53.57	27.78	$(\delta_{L1}, \delta_{A1}) = (1.5, 0.88)$, $(\delta_{L2}, \delta_{A2}) = (0.5, 1.19)$, $\delta_o = 2.43$
H_{41}	1.69	53.57	27.78	$(\delta_{L1}, \delta_{A1}) = (1.5, 1.27)$, $\delta_{o1} = 0.44$, $(\delta_{L2}, \delta_{A2}) = (0.52, 1.19)$, $\delta_{o2} = 1.90$
H_{42}	1.67	54.12	28.63	$(\delta_{L1}, \delta_{A1}) = (1.5, 1.36)$, $(\delta_{L2}, \delta_{A2}) = (1.5, 1.42)$, $(\delta_{L3}, \delta_{A3}) = (0.57, 1.16)$, $\delta_o = 3.55$

Nonlinear optimisation procedure considering high-frequency performance

Using a nonlinear model, further optimisations of H_{21} and H_{22} are performed in which the maximum $|K_{dyn}|$ is constrained to be no larger than that of the default mount. The default layout (H_1, only one inertia track) will also be refined as a baseline. Note the default value of the objective function, max($|T_d^*|$) (the * indicates the default system), is 3.45, and for the $|K_{dyn}^*|$, the default value is 701985 N/m.

Here a nonlinear orifice pressure-flow model (Bean 1971) is used, as expressed by

$$\Delta P = \frac{Q_o}{|Q_o|} \frac{\rho}{2K^2 A_o^2} Q_o^2, \tag{14}$$

where ρ is the fluid density, Q_o is the flow rate across the restriction, K represents flow coefficient and A_o is the orifice cross-section area. A diameter ratio $\beta = D_o/D_1$ is defined where D_o and D_1 are the orifice and upstream pipe diameters, respectively - D_o will be optimised here. In the relationship expressed by Equation (14), the flow is assumed to be steady, incompressible and symmetric along a streamline. For a standardised orifice, sufficient test data has been used to develop the empirical equations for predicting the empirical flow coefficient K based on specified restriction type, diameter ratio β and Reynolds number. In this analysis the concentric orifice case with corner pressure taps is considered and the empirical

equation for predicting K (Bean 1971) is

$$K = K_o(1 + b\lambda), \quad b = (0.002 + 0.026\beta^4)K_o, \quad \lambda = \frac{1000}{\sqrt{Re_{D1}}}, \quad Re_{D1} = \frac{\rho|\overline{V_1}|D_1}{\mu}, \tag{15}$$

$$K_o = 0.6004 + 0.35\beta^4 - 0.052(0.5 - \beta)^{(3/2)} - 0.62(\beta - 0.7)^{(5/3)}. \tag{16}$$

Re_{D1} is pipe Reynolds number, $\overline{V_1}$ is flow velocity in the upstream pipe and the dynamic viscosity μ is chosen as 0.02Ns/m^2 (Fan and Lu 2007). For the case in which the orifice is configured in the inertia track, a parameter constraint that $0.1 < \beta < 0.82$ is applied (Bean 1971) to ensure sufficient accuracy of Equations (15)-(16). If the inertia track and the orifice are configured in parallel, the upstream of the orifice will be the upper chamber which has a large cross-section area comparing with the orifice so variations of K are insensitive to Re_{D1}. In this case, a constant $K = 0.6$ is assumed in the calculation. Note that this model of predicting flow coefficient is not precise for all fluid conditions.

Nonlinear optimisation results

The nonlinear optimisation results are summarised in Table 4. In addition to Δ_d and Δ_{do}, Δ_k is added to represent the reduction of the max($|K_{dyn}|$) with optimal designs comparing with the default value. Table 4 shows that the optimal H_{21} configuration provides the maximum improvement of the objective function, 13.60% comparing with the optimal H_1. Also that the achieved max($|K_{dyn}|$) is much lower than the default system, a 28.63% reduction, which is beneficial for high-frequency isolation performance. Here more fluid flows through the orifice instead of the decoupler resulting in a smaller effective damping, hence a reduced $|K_{dyn}|$. The use of an orifice in H_{22} will reduce the low-frequency objective function value by 8.17% comparing with the optimised H_1. The $|T_d|$ and $|K_{dyn}|$ responses provided by beneficial designs are illustrated in Figure 3. It can be seen from this figure that the frequency locations of the max($|T_d|$) obtained with the beneficial configurations only slightly shift from the default one.

Table 4. Optimisation results using the nonlinear model and the high-frequency performance constraint.

Cases	Low frequency			High frequency	Parameter values
	Max($\|T_d\|$)	Δ_d (%)	Δ_{do}(%)	Max($\|K_{dyn}\|$), N/m (Δ_k)	
Default	3.45	-	-	701985	-
H_1	2.57	25.51	-	701985(0)	$(\delta_L, \delta_A) = (0.5, 0.51)$
H_{21}	1.97	42.90	13.60	500972.6(28.63%)	$(\delta_L, \delta_A) = (1.48, 1.05)$, $D_o = 5.4$ mm
H_{22}	2.36	31.60	8.17	701985(0)	$(\delta_L, \delta_A) = (0.98, 1.06)$, $D_o = 7.2$ mm

It can be seen from Table 4 that for H_{22} the optimal solution occurs at the maximum $|T_d|$ constraint. Therefore the sensitivity of the low-frequency max($|T_d|$) to the $|K_{dyn}|$ constraint is now considered. The variation in the $|K_{dyn}|$ constraint is represented by

$$\alpha_k = \frac{\max(|K_{dyn}|) - \max(|K^*_{dyn}|)}{\max(|K^*_{dyn}|)}. \tag{17}$$

Here α_k is set to be within [-0.5%, 2.0%]. For different constraint value, optimum tuning for both H_1 and H_{22}, where H_1 is used as a reference, are performed and the results are illustrated in Figure 4. It

can be seen that when α_k is increased from -0.5% to 2.0%, the improvement of low-frequency $|T_d|$ is compromised by high-frequency $|K_{dyn}|$, which suggests a trade-off between the two criteria. In addition, regardless of α_k, the optimised H_{22} configuration is always more beneficial than the optimised H_1 one. Note that the purpose of this sensitivity analysis is to illustrate a trade-off between the two criteria, rather than to discuss the exact variations of performance improvement.

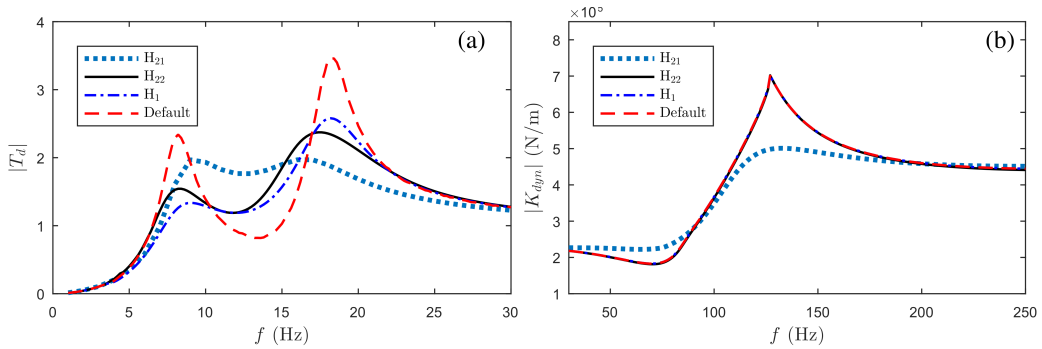

Figure 3. Shown are (a) $|T_d|$ frequency performances and (b) $|K_{dyn}|$ frequency responses with the default, H_1, H_{21} and H_{22} configurations.

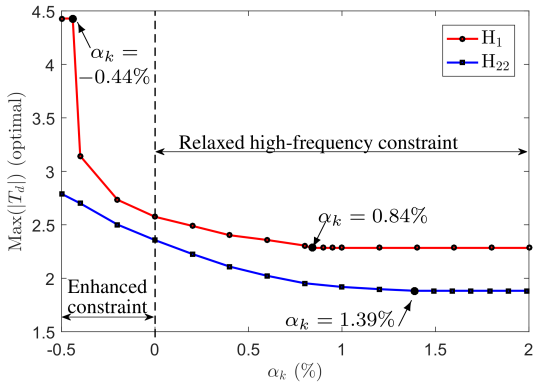

Figure 4. Sensitivity analysis of α_k on the optimised low-frequency max($|T_d|$) for H_1 and H_{22}.

Note that the optimal designs are obtained using a simplified model, which only includes the nonlinearities from the decoupler and the orifice while other parameters are assumed to be time-invariant. Some parameters, such as the inertia track resistance R_i, the upper chamber compliance C_1 and piston area A_p exhibit nonlinearity and are sensitive to the frequency and amplitude of the excitations (Geisberger et al. 2002). By conducting a numerical sensitivity analysis of cost functions to these parameter inaccuracies, it has been found that the optimal designs H_{21} and H_{22} are robust to small variations in the system parameters R_i, C_1 and A_p (Li 2018). Since only one typical excitation amplitude has been considered for low or high frequency excitation in the optimisations, to further investigate the

influence of excitation amplitude variations, further assessments have been carried out. It has been noticed that under different excitation amplitudes, the designs H_1, H_{21} and H_{22} still can provide improvements in terms of the low-frequency objective function while satisfying the high-frequency constraint. The percentage improvements are expected to be reduced due to the fact that the parameters in H_{21} and H_{22} are tuned for the optimum performance at the typical excitation amplitude. These results have not been included for the brevity of the paper.

Conclusion

This paper introduced a design methodology for the identification of beneficial fluid passageway configurations in a hydraulic engine mount. Via a numerical study, the performance advantages of new designs over a wide frequency range were investigated. Using a linearised low-frequency model excluding the effects of the decoupler, it was shown that the configurations consisting of a single inertia track and an orifice are beneficial in terms of reducing the maximum relative displacement transmissibility, over the optimum default system. Then investigations were extended to a model including the decoupler and orifice nonlinearities, and with a constraint on the high-frequency dynamic stiffness. A 13.6% improvement in the relative displacement transmissibility and a 28.6% reduction of the high-frequency maximum dynamic stiffness, over the optimum default system, were obtained, with the inertia track and orifice in series. In addition, using a configuration where the inertia track and orifice are in parallel, the percentage improvement on the cost function increases to 17.5% from 8.2%, with a marginal comprise on high-frequency dynamic stiffness. It has also been found that the optimal designs were robust to small parameter inaccuracies and excitation amplitudes. For a full industrial design process of an engine mount, more practical objective functions or constraints need to be considered, such as to consider a wider range of excitation amplitudes, to evaluate the actual frequency that the maximum transmissibility occurs, and to enhance the high-frequency performance. More accurate engine mount models can be employed to better assess the trade-off between the low and high frequency performances. It should be noted that the proposed methodology can be directly applied to other cost function, constraint and system models. A worthwhile extension of this work is to experimentally verify the performance advantages obtained in this analysis.

Declaration of conflicting interests

The author(s) declared no potential conflicts of interest with respect to the research, authorship, and/or publication of this article.

Funding

The author(s) disclosed receipt of the following financial support for the research, authorship, and/or publication of this article: This work was supported by the EPSRC with grant number EP/P013456/1 and EP/K005375/1.

References

Barszcz B, Dreyer JT and Singh R (2012) Experimental study of hydraulic engine mounts using multiple inertia tracks and orifices: Narrow and broad band tuning concepts. *Journal of Sound and Vibration* 331(24): 5209–5223.

Bean HS (1971) *Fluid meters: Their theory and application*, volume 2. American Society of Mechanical Engineers.

Colgate J, Chang C, Chiou Y, Liu W and Keer L (1995) Modelling of a hydraulic engine mount focusing on response to sinusoidal and composite excitations. *Journal of Sound and Vibration* 184(3): 503–528.

Fakhari V, Ohadi A and Talebi HA (2015) A robust adaptive control scheme for an active mount using a dynamic engine model. *Journal of Vibration and Control* 21(11): 2223–2245.

Fan R and Lu Z (2007) Fixed points on the nonlinear dynamic properties of hydraulic engine mounts and parameter identification method: experiment and theory. *Journal of Sound and Vibration* 305(4-5): 703–727.

Foumani MS, Khajepour A and Durali M (2004) A new high-performance adaptive engine mount. *Modal Analysis* 10(1): 39–54.

Geisberger A, Khajepour A and Golnaraghi F (2002) Non-linear modelling of hydraulic mounts: Theory and experiment. *Journal of Sound and Vibration* 249(2): 371–397.

Guo R, Wei XK, Zhou SQ and Gao J (2017) Parametric identification study of an active engine mount: Combination of finite element analysis and experiment. *Proceedings of the Institution of Mechanical Engineers, Part D: Journal of Automobile Engineering* .

He S and Singh R (2007) Discontinuous compliance nonlinearities in the hydraulic engine mount. *Journal of Sound and Vibration* 307(3-5): 545–563.

Kim G and Singh R (1995) A study of passive and adaptive hydraulic engine mount systems with emphasis on non-linear characteristics. *Journal of Sound and Vibration* 179(3): 427–453.

Li Y (2018) *Optimal Design Methodologies for Passive Vibration Suppression*. PhD Thesis, University of Bristol.

Mansour H, Arzanpour S and Golnaraghi M (2011) Active decoupler hydraulic engine mount design with application to variable displacement engine. *Journal of Vibration and Control* 17(10): 1498–1508.

Marzbani H, Jazar RN and Fard M (2014) Hydraulic engine mounts: a survey. *Journal of Vibration and Control* 20(10): 1439–1463.

Singh R, Kim G and Ravindra P (1992) Linear analysis of automotive hydro-mechanical mount with emphasis on decoupler characteristics. *Journal of Sound and Vibration* 158(2): 219–243.

Smith MC (2002) Synthesis of mechanical networks: The inerter. *IEEE Transactions on Automatic Control* 47(10): 1648–1662.

Tikani R, Vahdati N, Ziaei-Rad S and Esfahanian M (2011) A new hydraulic engine mount design without the peak frequency. *Journal of Vibration and Control* 17(11): 1644–1656.

Tiwari M, Adiguna H and Singh R (2003) Experimental characterization of a nonlinear hydraulic engine mount. *Noise Control Engineering Journal* 51(1): 36–49.

Truong TQ and Ahn KK (2010) A new type of semi-active hydraulic engine mount using controllable area of inertia track. *Journal of Sound and Vibration* 329(3): 247–260.

Wang LR, Lu ZH and Hagiwara I (2010) Analytical analysis approach to nonlinear dynamic characteristics of hydraulically damped rubber mount for vehicle engine. *Nonlinear Dynamics* 61(1-2): 251–264.

Wang M, Yao GF, Zhao JZ and Qin M (2014) A novel design of semi-active hydraulic mount with wide-band tunable notch frequency. *Journal of Sound and Vibration* 333(8): 2196–2211.

Zhang SY, Jiang JZ and Neild SA (2017) Passive vibration control: a structure–immittance approach. *Proceedings of the Royal Society A* 473(2201): 20170011.

Zhang YQ and Shangguan WB (2006) A novel approach for lower frequency performance design of hydraulic engine mounts. *Computers & Structures* 84(8): 572–584.